Sheetal Gonsalves[*], *Swapna Gabbur*

ENHANCING CONVECTIVE HEAT TRANSFER IN ENGINE OIL: A COMPARATIVE STUDY OF VARIOUS NANOPARTICLES

POBOLJŠANJE PRENOSA TOPLOTE KONVEKCIJOM U MOTORNOM ULJU: UPOREDNA STUDIJA RAZLIČITIH NANOČESTICA

Originalni naučni rad / Original scientific paper
Rad primljen / Paper received: 16.07.2024
https://doi.org/10.69644/ivk-2025-siA-0009

Author's address:
Department of Basic Science and Humanities, Mukesh Patel School of Technology Management & Engineering, SVKM's Narsee Monjee Institute of Management Studies (NMIMS) Deemed-to-University, Mumbai-400056, India
[*] sheetal.gonsalves@nmims.edu

Keywords
- nanofluid
- convective boundary condition
- FEM
- engine oil
- flat plate

Ključne reči
- nanofluid
- granični uslov konvekcije
- MKE
- motorno ulje
- ravna ploča

Abstract

The study explores heat transfer properties of five different nanofluid flows past an oil cooling system. The numerical investigation is carried out by developing mathematical model by utilising nanofluids volume fraction in engine oil based nanofluid containing solid particles of molybdenum disulfide (MoS_2), aluminium oxide (Al_2O_3), titanium oxide (TiO_2), graphene oxide (GO), and copper (Cu). The system of PDE is converted to ODE using appropriate similarity transformations and then solved by employing the FEM. The influence of different nanoparticles on temperature and velocity distributions are analysed graphically. Additionally, the impact of various nanoparticles for the key parameters on the rate of heat transfer and coefficient of skin friction are presented in tabular form. The GO nanoparticles suspended in engine oil exhibit the comparatively lowest temperature and skin friction coefficient, and highest heat transfer capabilities. It may therefore be considered as the best lubricant for engines as it offers low friction and temperature, potentially extending the engine component's lifespan.

Izvod

U radu se izučavaju karakteristike prenosa toplote kod pet različitih protoka nanofluida u sistemu za hlađenje ulja. Numerički deo istraživanja se izvodi razvojem matematičkog modela korišćenjem zapreminskog udela nanofluida u motornom ulju na bazi nanofluida, koje sadrži čvrste čestice molibden disulfida (MoS_2), aluminijum oksida (Al_2O_3), titanijum oksida (TiO_2), grafen oksida (GO) i bakra (Cu). Sistem PDJ se prevodi u ODJ primenom odgovarajućih transformacija sličnosti, a zatim se rešavaju MKE. Uticaj različitih nanočestica se proučavaju sa raspodelom temperature i brzine, gde se analiza izvodi grafički. Osim toga, tabelarno je predstavljen uticaj raznih nanočestica prema ključnim parametrima brzine prenosa toplote i koeficijenta trenja strujanja. Nanočestice GO suspendovane u motornom ulju pokazuju uporedivo najnižu temperaturu i koeficijent trenja strujanja, kao i najbolje osobine prenosa toplote. Stoga se može smatrati da kao najbolje sredstvo podmazivanja motora, jer obezbeđuje nisko trenje i nižu temperaturu, potencijalno produžavajući vek komponenata motora.

INTRODUCTION

In recent decades, nanotechnology has emerged as a focal point in various engineering domains, particularly in fluid cooling and heating owing to their exceptional thermal conductivity and rheological properties. Choi and Eastman /1/ introduced the term ‘nanofluid’ to explain fluids infused with nanoparticles ranging from 1 to 100 nanometres in size. Initial research by Masuda et al. /2/ emphasized enhancement of thermal conductivity using ultra-fine particles, with subsequent studies revealing that maintaining a minimum of 5 % nanoparticles volume fraction enhances the thermal characteristics of nanofluid, /3/. Applications of nanofluids extend across diverse fields such as power, transportation, manufacturing, and electronic devices. Beyond traditional engineering applications, nanofluids demonstrate promise in space technology /4/, combustion processes /5/, supercapacitors /6/, and nano-solar collectors /7/. Assael et al. /8/ outlined numerous potential applications for nanofluids in heat transfer. With advancements in automotive technology, the demand for high-efficiency engines has surged. These engines offer superior performance and boast improved fuel economy and reduced emissions. This trend reflects a growing emphasis on sustainability and efficiency in the automotive industry, driving manufacturers to develop innovative solutions to meet consumer and regulatory demands, /9/. The increased demand for high-efficiency engines in the automotive industry has led to the utilisation of engine oil base nanoparticles which play a crucial role in enhancing efficiency and performance by reducing friction, minimising wear, improving thermal stability, and contributing to better fuel economy, /10/.

Traditional fluids such as ethylene glycol, kerosene oil, engine oil, and water are commonly employed in heat transfer applications, yet their effectiveness is hindered by their

limited thermal conductivity. Nanofluids ability to save energy and lower equipment temperatures through enhanced thermal performance has garnered significant attention across industries and academia, /11-15/. Lee et al. /16/ research reveals a direct relationship between volume fraction and thermal conductivity, emphasizing the pivotal role of volume fraction in nanofluid analysis. Hwang et al. /17/ experimentally studied Al_2O_3·H_2O flow past a circular tube considering convective heat transfer and constant heat flux. Godson et al. /18/ conducted experiments using silver-water nanofluid to examine the convective heat transfer properties at volume concentrations of 0.3 %, 0.6 %, and 0.9 %. Abdel-Gaied and Hamad /19/ found that suspending alumina nanoparticles in a fluid enhances the base fluid heat transfer capacity, especially when considering a moving vertical plate under a magnetic effect. Vasanthakumari /20/ studied the effect of water-based Ag and TiO_2 nanofluid flow over a stretched surface numerically. Khan and Alqahtani /21/ numerically proved that velocity and temperature distributions are significantly affected by the volume fraction for Ag-ethylene glycol and Ag-water nanofluid in a channel. Elgazery /22/ employs the Chebyshev pseudospectral technique to investigate Casson magneto-nanofluid flow, utilising Al_2O_3 and Au nanoparticles with blood and water as base fluids. Mahalakshmi and Vennila /23/ utilised the Adomian Decomposition Method to investigate the flow of nanofluids consisting of Au-water and Ag-water across a plate. Klazly and Bognár /24/ investigated the laminar flow over a flat plate of Fe_3O_4, TiO_2, and Al_2O_3 nanofluids of 1, 2, 3, and 4 % volume fractions. Many researchers have been investigating GO and MoS_2 owing to their remarkable properties such as excellent optical, magnetic, and thermal stability. Aminuddin et al. /25/ examined the influence of the slip on a shrinking Riga plate using glycerine-based GO and MoS_2 nanoparticles. In recent times, numerous studies have indicated the significance of nanoparticle volume fraction in investigating the heat and mass transport of nanofluids /26-29/.

Engine oil is used as a lubricant in various industries such as production, chemical, and mechanical /30/. The outcomes of graphene-engine oil nanofluid are examined by Eswaraiah et al. /31/. Meng et al. /32/ investigated tribological properties of Ag-engine oil nanofluid. Using the Laplace transform method for nanofluid flow of graphene-engine oil, Aman et al. /33/ provided an exact solution for flow over a flat plate. Arif et al. /34/ investigated the impact of graphene and MoS_2 considering engine oil as base fluid. The flow of MoS_2 Casson nanofluid with an engine oil base, under ramped boundary conditions and thermal radiation, within a channel was investigated by Siddique et al. /35/. Recently, Le et al. /36/ applied a fractional approach to study the flow of engine oil-based nanofluid considering MoS_2 and graphene nanoparticles over a vertical plate.

These investigations underscore the increased heat transfer capabilities facilitated by the presence of nanoparticles within the base fluid. According to existing research, the thermal capabilities of engine oil can be enhanced by suspending different nanoparticles. The objective of the work is to present a comparative study of the flow and heat transfer for GO, MoS_2, Al_2O_3, TiO_2, and Cu nanoparticles taking engine oil as base fluid. In this study, FEM is employed to analyse the hydraulic and thermal behaviour of engine oil nanofluid flow over a flat plate subjected to convective boundary condition by simulating oil cooling systems in modern engines. We explore five different types of nanoparticles dispersed in engine oil and vary their volume fractions from 1 to 4 %. The effect of various types of nanoparticles on temperature and velocity distributions are portrayed graphically and discussed. The numerical values of rate of heat transfer and coefficient of skin friction for various key parameters and different nanoparticles are analysed by presenting in tabular form.

NUMERICAL ANALYSIS

Model formulation

Consider incompressible, laminar, steady engine oil nanofluid flow through oil cooling system with T_∞ and U_∞ as ambient temperature and velocity, respectively. The surface of the oil cooling system is assumed as a vertical flat plate having temperature T_w and constant mass flux velocity S_w and convectively heated by the fluid of temperature T_f as shown in Fig. 1.

The basic equations /37/ can be written as

$$u_x + v_y = 0\,, \tag{1}$$

$$\rho_{nf}\,(uu_x + vu_y) = \mu_{nf}\,u_{yy}\,, \tag{2}$$

$$(\rho C_p)_{nf}\,(uT_x + vT_y) = k_{nf}\,(T_{yy})\,, \tag{3}$$

corresponding boundary constraints are

$$y = 0:\ u = 0,\ v = S_w(x),\ -k_{nf}T_y = h_f\,[T_f - T_w]$$

$$y \to \infty:\ u \to U_\infty,\ T \to T_\infty\,. \tag{4}$$

Introducing similarity variables

$$f(\eta) = \frac{\Psi(x,y)}{\sqrt{U_\infty \nu_f\, x}},\ \ \eta = y\sqrt{\frac{U_\infty}{\nu_f\, x}},\ \ \theta(\eta) = \frac{T - T_\infty}{T_f - T_\infty}\,, \tag{5}$$

where: $u = \Psi_y$, $v = -\Psi_x$, so that it satisfies Eq.(1).

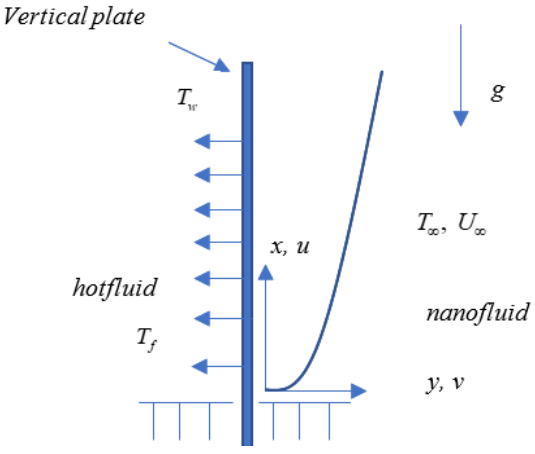

Figure 1. Geometry of flat plate used as oil cooling system.

From Eq.(5), we have

$$\Psi(x,y) = \sqrt{U_\infty \nu_f\, x}\, f(\eta)\,, \tag{6}$$

$$u = U_\infty f'(\eta),\ \ v = -\frac{1}{2}(U_\infty \nu_f)^{1/2}\,(f(\eta) - \eta f'(\eta))x^{-1/2}, \tag{7}$$

$$S_w(x) = -\frac{1}{2}\left(\frac{U_\infty \nu_f}{x}\right)^{1/2} s_w . \quad (8)$$

Using Eq.(5) in Eqs. (2) and (3) we get the system of nonlinear ODE

$$2f''' + \left[1-\phi+\phi\left(\frac{\rho_s}{\rho_f}\right)\right](1-\phi)^{2.5} f'' f = 0 , \quad (9)$$

$$\left(\frac{k_{nf}}{k_f}\right)\theta'' + \frac{1}{2}\mathrm{Pr}\left[1-\phi+\phi\frac{(\rho C_p)_s}{(\rho C_p)_f}\right] f\theta' = 0 , \quad (10)$$

with boundary constraints

$$f(0) = s_w,\ f'(0) = 0,\ \theta'(0) = -a[1-\theta(0)],$$
$$f'(\infty) \to 1,\ \theta(\infty) \to 0 . \quad (11)$$

Dimensionless parameters are given by Prandtl number $\mathrm{Pr} = \frac{\mu_f (C_p)_f}{k_f}$, local Reynolds number $\mathrm{Re}_x = \frac{U_\infty x}{\nu_f}$, convective boundary parameter $a = \frac{c}{k_{nf}}\left(\frac{\nu_f}{U_\infty}\right)^{1/2}$, and suction parameter s_w is given by Eq.(8).

The skin friction coefficient c_f, local Nusselt number Nu_x are of practical interest and are defined as

$$c_f = \frac{\tau_w}{\frac{1}{2}\rho_f U_\infty^2},\ Nu_x = \frac{x q_w}{k_f (T_f - T_\infty)}, \quad (12)$$

where: heat flux q_w; shear stress τ_w are given by

$$q_w = -k_{nf}(T_y)_{y=0},\ \tau_w = \mu_{nf}(u_y)_{y=0} . \quad (13)$$

Using Eq.(5) in Eq. (12) and (13), we get

$$\frac{Nu_x}{(\mathrm{Re}_x)^{1/2}} = -\left[\frac{k_{nf}}{k_f}\right]\theta'(0),\ c_f(\mathrm{Re}_x)^{1/2} = \frac{f''(0)}{(1-\phi)^{2.5}}, \quad (14)$$

Characteristics of nanofluid

The nanofluid physical properties are characterised with the volume fraction of nanoparticles as follows /38, 39/

density: $\rho_{nf} = \phi\rho_s - (\phi-1)\rho_f$,

thermal conductivity: $\frac{k_{nf}}{k_f} = \frac{2\phi(k_s-k_f)+k_s+2k_f}{\phi(k_f-k_s)+k_s+2k_f}$,

heat capacity: $(\rho C_p)_{nf} = \phi(\rho C_p)_s + (1-\phi)(\rho C_p)_f$,

viscosity: $\mu_{nf} = (1-\phi)^{-2.5}\mu_f$.

Thermophysical properties of nanoparticles and engine oil are presented in Table 1.

Table 1. Thermophysical properties of nanoparticles and engine oil.

Nanoparticle	k (W/mK)	C_p (J/kgK)	ρ (kg/m^3)
GO	5000	2100	2500
TiO_2	8.9538	686.2	4250
Al_2O_3	40	765	3970
MoS_2	904.4	397.21	5060
Cu	401	385	8933
Engine oil (base fluid)	0.144	1910	884

Solution procedure

Finite element modelling

The system of nonlinear ODE given by Eqs. (9)-(10) with Eq.(11) are solved by employing FEM, using quadratic interpolation functions. The methodology employed in this context is elucidated in the work by Reddy /40/. Further insights into the FEM can be found in our earlier publications /28, 29/.

Variational formulation

The variational form associated with Eqs. (9)-(10) for a standard element (η_e, η_{e+1}) is articulated as

$$\int_{\eta_e}^{\eta_{e+1}} w_1(f'-q)d\eta = 0 , \quad (15)$$

$$\int_{\eta_e}^{\eta_{e+1}} w_2\left[2q'' + (1-\phi)^{2.5}\left(1-\phi+\phi\left(\frac{\rho_s}{\rho_f}\right)\right) f q'\right] d\eta = 0 , \quad (16)$$

$$\int_{\eta_e}^{\eta_{e+1}} w_3\left[\frac{1}{\mathrm{Pr}}\left(\frac{k_{nf}}{k_f}\right)\theta'' + \frac{1}{2}\left(1-\phi+\phi\frac{(\rho C_p)_s}{(\rho C_p)_f}\right) f\theta'\right] d\eta = 0 . \quad (17)$$

Here, w_i (i = 1, 2, 3) are arbitrary test functions. Functions f, q and θ are approximated by the quadratic polynomials ψ_I (i = 1, 2, 3).

Finite element formulation

Taking $w_1 = w_2 = w_3 = \psi_I$ (i = 1, 2, 3) with $f = \sum_{j=1}^{3} f_j\psi_j$, $q = \sum_{j=1}^{3} q_j\psi_j$, $\theta = \sum_{j=1}^{3}\theta_j\psi_j$, and quadratic interpolation functions for $\eta_e \le \eta_1 \le \eta_{e+1}$ are

$$\psi_1 = (\eta_{e+1}+\eta_e-2\eta_1)(\eta_{e+1}-\eta_1)(\eta_{e+1}-\eta_e)^{-2},$$
$$\psi_2 = 4(\eta_1-\eta_e)(\eta_{e+1}-\eta_1)(\eta_{e+1}-\eta_e)^{-2},$$
$$\psi_3 = (\eta_{e+1}+\eta_e-2\eta_1)(\eta_1-\eta_e)(\eta_{e+1}-\eta_e)^{-2} .$$

From Eqs.(15)-(17), the finite element model is

$$\begin{bmatrix} [K^{11}] & [K^{12}] & [K^{13}] \\ [K^{21}] & [K^{22}] & [K^{23}] \\ [K^{31}] & [K^{32}] & [K^{33}] \end{bmatrix}\begin{Bmatrix} \{f\} \\ \{q\} \\ \{\theta\} \end{Bmatrix} = \begin{Bmatrix} \{r^1\} \\ \{r^2\} \\ \{r^3\} \end{Bmatrix}, \quad (18)$$

where: $[K^{mn}]$ are 2×2, and $\{r^m\}$ are 2×1 order matrices (m, n = 1, 2, 3) and are given by

$$K_{ij}^{11} = \int_{\eta_e}^{\eta_{e+1}} \psi_i \frac{d\psi_j}{d\eta} d\eta,\ K_{ij}^{12} = -\int_{\eta_e}^{\eta_{e+1}} \psi_i\psi_j d\eta,\ K_{ij}^{13} = 0,\ K_{ij}^{21} = 0,$$

$$K_{ij}^{23} = 0,\ K_{ij}^{22} = -2\int_{\eta_e}^{\eta_{e+1}} \frac{d\psi_i}{d\eta}\frac{d\psi_j}{d\eta} d\eta + \left(\left[1-\phi+\phi\left(\frac{\rho_s}{\rho_f}\right)\right](1-\phi)^{2.5}\right)\times$$
$$\times \int_{\eta_e}^{\eta_{e+1}} \bar{f}\psi_i \frac{d\psi_j}{d\eta} d\eta,\ K_{ij}^{33} = -\int_{\eta_e}^{\eta_{e+1}} \frac{d\psi_i}{d\eta}\frac{d\psi_j}{d\eta} d\eta +$$
$$+\left[\frac{1}{2}\mathrm{Pr}\left(\frac{k_f}{k_{nf}}\right)\left(1-\phi+\phi\frac{(\rho C_p)_s}{(\rho C_p)_f}\right)\right]\int_{\eta_e}^{\eta_{e+1}} \bar{f}\psi_i \frac{d\psi_j}{d\eta} d\eta ,$$

$$K_{ij}^{31} = 0,\ K_{ij}^{32} = 0,\ r_i^1 = 0,\ r_i^2 = -\left[\psi_i \frac{dq}{d\eta}\right]_{\eta_e}^{\eta_{e+1}},\ r_i^3 = -\left[\psi_i \frac{d\theta}{d\eta}\right]_{\eta_e}^{\eta_{e+1}}$$

where: $\bar{f} = \sum_{i=1}^{3} \bar{f}_i\psi_i$ is assumed to be known. The $\bar{f}$ is employed to linearize the nonlinear FEM model. By carrying convergence analysis, element size is fixed as 450. To get accurate numerical results, η is fixed at 10. After applying boundary conditions, the remaining system of 1499 equations

is solved for f, q, and θ using iterative scheme. When $\sum_{i,j}\left|\Delta^{n^*+1}-\Delta^{n^*}\right|\leq 10^{-8}$ is satisfied, the iterative procedure is terminated. Here iterative steps are denoted by n^* and $\Delta = f, q, \theta$.

Code verification

The accuracy of the novel FEM code formulated in the study is validated by comparing the numerical results with published data for the Newtonian fluid ($\phi = 0$) and presented in Table 2. An excellent correlation is achieved, thus validating the FEM code.

Table 2. Computed values of $-\theta'(0)$ for different Pr when $s_w = 0$, $a \to \infty$, $\phi = 0$.

Pr	Roşca and Pop /41/	Present result
0.7	0.29268	0.292682
0.8	0.30691	0.306907
1	0.33205	0.332053
5	0.57668	0.576680
10	0.72814	0.728144
30	-	1.051336
50	-	1.247329

RESULTS AND DISCUSSION

The present study investigates the impact of five different types of nanoparticles, namely GO, MoS_2, Al_2O_3, TiO_2, and Cu dispersed in engine oil, on steady laminar flow over a flat surface. The velocity and temperature profiles for these five nanoparticles suspended in engine oil are compared graphically in Figs. 2-4. Tables 3-7 present the variation of $f''(0)$ and $-\theta'(0)$ for various values of ϕ, s_w, and a, for engine oil-based five different nanoparticles. Finally, Table 8 presents the effect of Pr on $-\theta'(0)$ and $\theta(0)$. The default values are Pr = 60, $\phi = 0.02$, $a = 10$, and $s_w = 0.5$ unless otherwise indicated.

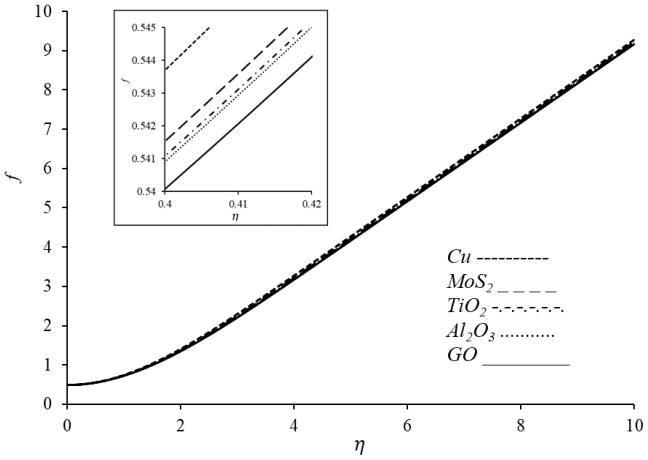

Figure 2. Primary velocity profile for GO, MoS_2, Al_2O_3, TiO_2, and Cu.

The comparison of primary and secondary velocity profiles for engine oil-based nanofluid employing five different types of nanoparticles are portrayed in Fig. 2 and Fig. 3 respectively. As illustrated in the figures, Cu exhibits the thinnest velocity boundary layer followed by MoS_2 and GO has the thickest boundary layer among all the nanoparticles under study, while the boundary layer thickness for Al_2O_3 is slightly greater than that of TiO_2. Nanoparticles like Cu and MoS_2 may reduce the thickness of the boundary layer and elevate velocity, while nanoparticles like GO may augment the thickness of the boundary layer and diminish velocity compared to engine oil. Thus, lower velocity results in reduced velocity gradient and consequently lowers the skin friction.

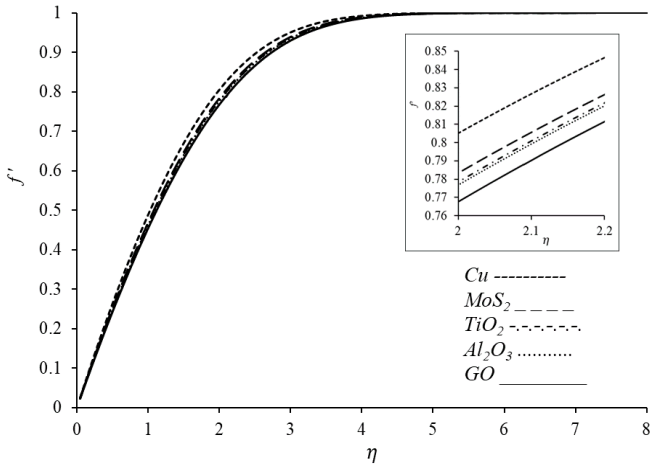

Figure 3. Secondary velocity profile for GO, MoS_2, Al_2O_3, TiO_2, and Cu.

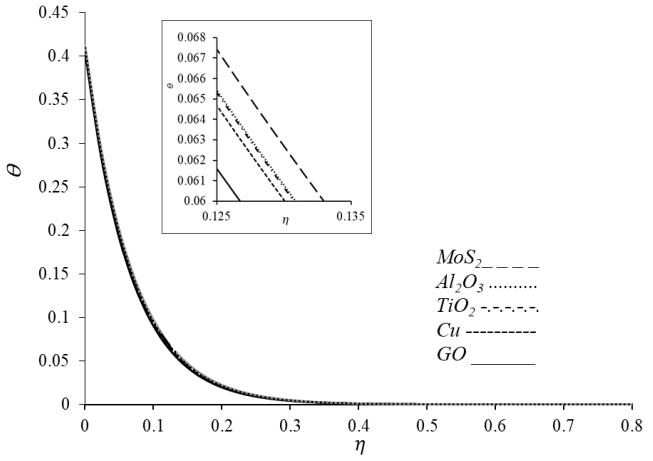

Figure 4. Temperature profile for GO, MoS_2, Al_2O_3, TiO_2, and Cu.

Figure 4 presents a comparison of temperature profiles for engine oil-based nanofluids utilising five different types of nanoparticles. It is observed that MoS_2 nanoparticle has the thickest thermal boundary layer followed by Al_2O_3, TiO_2, Cu and GO, respectively. Nanoparticles such as MoS_2 lead to an increase in the thickness of the boundary layer and wall temperature, while nanoparticles like GO demonstrate opposite trends compared to the base fluid. This effect offers significant benefits across various applications where efficient heat transfer and thermal management are essential.

Values of $f''(0)$ for engine oil-based five different nanoparticles varying ϕ from 1 to 4 % are illustrated in Table 3. As ϕ increases, the value of $f''(0)$ increases for Cu, MoS_2, TiO_2, Al_2O_3, whereas for GO it decreases. It is observed that the values of $f''(0)$ for Cu nanoparticles suspended in engine oil are highest while GO has lowest values among the other nanoparticles under study. It is noteworthy that, for GO nanoparticles, the value of $f''(0)$ declines as ϕ increases up to 4 %. Nanoparticles like GO can be incorporated into lubricants to modify boundary layer characteris-

tics and decrease drag, resulting in enhanced hydrodynamic performance.

Table 4 demonstrates comparison among Cu, MoS_2, TiO_2, Al_2O_3, and GO with various ϕ for the values of $-\theta'(0)$. As ϕ increases, the value of $-\theta'(0)$ decreases. GO nanoparticles exhibit the highest values of $-\theta'(0)$, followed by Cu, TiO_2, and Al_2O_3, respectively. For MoS_2 nanoparticles, $-\theta'(0)$ is the minimum among other nanoparticles under study, aligning with the trends observed in Fig. 4, indicating a more gradual gradient of temperature for MoS_2-engine oil nanofluid. Therefore, incorporating MoS_2 nanoparticles in engine oil ensures optimal engine performance and durability by stabilising temperature and reducing temperature gradient, thus minimising wear and risk of overheating.

The values of $-\theta'(0)$ for engine oil-based Cu, MoS_2, TiO_2, Al_2O_3, and GO nanoparticles by varying a is presented in Table 5. It is observed that, as a increases, $-\theta'(0)$ increases. A 50 % average enhancement in the values of $-\theta'(0)$ is observed for all types of nanoparticles when values of a vary from 0 to 20. Therefore, convective boundary parameter directly influences heat transfer efficiency and plays a key role in designing efficient cooling systems for engines.

Tables 6 and 7 provide values $f''(0)$ and $-\theta'(0)$ for engine oil-based five different nanoparticles for different values of s_w, respectively. From Table 7, it is observed that as s_w increases, $f''(0)$ increases. By varying the value of s_w between 0.1 to 1, a 31 % average enhancement in the values of $f''(0)$ is observed for all types of nanoparticles. When suction is applied, GO nanoparticles demonstrate the lowest values of $f''(0)$, followed by Al_2O_3, TiO_2, MoS_2, and Cu which exhibit increasing values, respectively. The values of $-\theta'(0)$ increase with increase in s_w as seen in Table 7. An average 73 % enhancement is noted in the values of $-\theta'(0)$ when varying s_w from 0.1 to 1. Under the effect of suction, GO nanoparticles exhibit the highest value of $-\theta'(0)$, followed by Cu, TiO_2, Al_2O_3, and MoS_2, respectively. Thus, suction parameter is significant for optimising the performance of engine oil nanofluid in cooling systems.

Table 8 proposes the solution for heat transfer coefficient $-\theta'(0)$ and wall temperature $\theta(0)$ corresponding to different Pr. It is observed that as Pr rises, $-\theta'(0)$ increases while $\theta(0)$ decreases. Physically, a fluid with a high Prandtl number (Pr), such as engine oil, tends to have a lower temperature at its surface because it has a greater capacity to resist changes in temperature. However, despite the lower surface temperature, it exhibits a high heat transfer rate due to its ability to efficiently transfer heat throughout the fluid. This characteristic makes engine oil an effective fluid for safeguarding the surface of engine components against heat damage, while offering effective lubrication.

Table 3. Effect of volume fraction on $f''(0)$.

	ϕ	Cu	MoS_2	TiO_2	Al_2O_3	GO
$f''(0)$	0.01	0.545778	0.530485	0.52727	0.526157	0.520303
	0.02	0.567006	0.537417	0.531167	0.529001	0.517586
	0.03	0.586616	0.543648	0.534536	0.531375	0.514682
	0.04	0.604698	0.549206	0.537394	0.533293	0.511598

Table 4. Effect of volume fraction on $-\theta'(0)$.

	ϕ	GO	Cu	TiO_2	Al_2O_3	MoS_2
$-\theta'(0)$	0.01	5.868914	5.846965	5.842942	5.842148	5.828621
	0.02	5.849422	5.805949	5.797903	5.79632	5.769145
	0.03	5.82954	5.764964	5.752902	5.750533	5.709613
	0.04	5.809267	5.723999	5.707936	5.704782	5.650047

Table 5. Effect of convective boundary parameter on $-\theta'(0)$.

	a	GO	Cu	TiO_2	Al_2O_3	MoS_2
$-\theta'(0)$	5	3.663363	3.647226	3.644201	3.643608	3.633412
	10	5.849422	5.805949	5.797903	5.79632	5.769145
	20	8.336877	8.246389	8.22978	8.226509	8.170455

Table 6. Effect of suction parameter on $f''(0)$.

	s_w	GO	Al_2O_3	TiO_2	MoS_2	Cu
$f''(0)$	0.1	0.36573	0.372141	0.373353	0.376843	0.393212
	0.5	0.517586	0.529001	0.531167	0.537417	0.567006
	1	0.720497	0.738717	0.74218	0.752186	0.799777

Table 7. Effect of suction parameter on $-\theta'(0)$.

	s_w	GO	Cu	TiO_2	Al_2O_3	MoS_2
$-\theta'(0)$	0.1	2.578434	2.560247	2.545365	2.543679	2.526919
	0.5	5.849422	5.805949	5.797903	5.79632	5.769145
	1	7.013365	6.990513	6.986532	6.985711	6.971156

Table 8. Results for $-\theta'(0)$ and $\theta(0)$ by varying Pr when $\phi = 0$, $s_w = 0$, $a = 1$.

Pr	$-\theta'(0)$	$\theta(0)$
0.7	0.226416	0.773584
0.8	0.234843	0.765157
1	0.249284	0.750715
5	0.365770	0.634230
10	0.421362	0.578640
30	0.512639	0.487368
50	0.555079	0.444933

CONCLUSIONS

A comparative study of various nanofluid flows considering GO, MoS_2, Al_2O_3, TiO_2, and Cu nanoparticles, and taking engine oil as base fluid is presented in this work. The key parameters considered for the study are nanoparticles volume fraction, convective boundary, and suction parameter. Numerical solutions for the transformed dimensionless boundary layer equations are computed using FEM. The following key findings are observed.

The velocity profiles of the Cu-engine oil nanofluid are greater, while GO-engine oil has lowest profiles among the studied nanofluids.

The GO-engine oil nanofluid has lowest skin friction coefficient which aids in reducing drag and friction forces.

Temperature distribution within the boundary layer of MoS_2-engine oil is observed to be higher compared to TiO_2, Al_2O_3, Cu, and GO nanoparticles. The increase in the thermal boundary layer with MoS_2-infused lubricants may offer opportunities for improving thermal management, reducing friction and wear, and enhancing the performance and reliability of machinery and equipment across various industrial applications.

The altered boundary layer thickness of GO-engine oil results in improved heat transfer rates, leading to better thermal performance in cooling systems.

REFERENCES

1. Choi, S.U.S., Eastman, J.A. (1995), *Enhancing thermal conductivity of fluids with nanoparticles*, Int. Mech. Eng. Congress and Exhibition, San Francisco, CA (USA), 1995, DOE Contract No. W-31109-ENG-38, OSTI ID 196525, Argonne National Lab (ANL), Argonne, IL, USDOE, Washington, DC.
2. Masuda, H., Ebata, A., Teramae, K., Hishinuma, N. (1993), *Alteration of thermal conductivity and viscosity of liquid by dispersing ultra-fine particles, Dispersion of Al_2O_3, SiO_2 and TiO_2 ultra-fine particles*, Netsu Bussei, 7(4): 227-233. doi: 10.2963/JJTP.7.227
3. Godson, L., Raja, B., Lal, D.M., Wongwises, S.E. (2010), *Enhancement of heat transfer using nanofluids-An overview*, Renew. Sust. Energy Rev. 14(2): 629-641. doi: 10.1016/j.rser.2009.10.004
4. Ungar, E., Erickson, L. (2011), *Assessment of the use of nanofluids in spacecraft active thermal control systems*, In: AIAA SPACE 2011 Conference & Exposition, Long Beach, CA, 2011: 7328. doi: 10.2514/6.2011-7328
5. Allen, C., Mittal, G., Sung, C.-J., et al. (2011), *An aerosol rapid compression machine for studying energetic-nanoparticle-enhanced combustion of liquid fuels*, Proc. Comb. Inst. 33(2): 3367-3374. doi: 10.1016/j.proci.2010.06.007
6. Arun, T., Prabakaran, K., Udayabhaskar, R., et al. (2019), *Carbon decorated octahedral shaped Fe_3O_4 and α-Fe_2O_3 magnetic hybrid nanomaterials for next generation supercapacitor applications*, Appl. Surf. Sci. 485: 147-157. doi: 10.1016/j.apsusc.2019.04.177
7. Balakin, B.V., Stava, M., Kosinska, A. (2022), *Photothermal convection of a magnetic nanofluid in a direct absorption solar collector*, Solar Energy, 239: 33-39. doi: 10.1016/j.solener.2022.04.027
8. Assael, M.J., Antoniadis, K.D., Wakeham, W.A., Zhang, X. (2019), *Potential applications of nanofluids for heat transfer*, Int. J Heat Mass Transfer, 138: 597-607. doi: 10.1016/j.ijheatmasstransfer.2019.04.086
9. Manikandan, S., Jancirani, J. (2014), *Review on heat transfer enhancement of nanofluids - engine coolant*, Adv. Mater. Res. 984-985: 1095-1101. doi: 10.4028/www.scientific.net/AMR.984-985.1095
10. Kim, B.-K., Hyun, J.-S., Kim, Y.H., et al. (2023), *Effect of boundary layer modification and enhanced thermal characteristics on tribological performance of alumina nanofluids dispersed in lubricant oil*, Exp. Tech. 47(3): 737-746. doi: 10.1007/s40799-022-00588-z
11. Singh, P. (2018), *Heat transfer characteristics of propylene glycol/water based magnesium oxide nanofluid flowing through straight tubes and helical coils*, J Therm. Eng. 4(1): 1737-1755. doi: 10.18186/journal-of-thermal-engineering.369007
12. Sheikholeslami, M., Zareei, A., Jafaryar, M., et al. (2019), *Heat transfer simulation during charging of nanoparticle enhanced PCM within a channel*, Physica A: Stat. Mech. Appl. 525: 557-565. doi: 10.1016/j.physa.2019.03.082
13. Sundari, K.G., Asirvatham, L.G., Marshal S, J.J., et al. (2020), *Feasibility of glycerin/Al_2O_3 nanofluid for automotive cooling applications*, J Ther. Eng. 6(4): 619-632. doi: 10.18186/thermal.766416
14. Hossain, F., Miah, A., Morshed, A., et al. (2021), *Investigation of laminar forced convection heat transfer of nanofluids through flat plate solar collector*, J Ther. Eng. 7 (Supp 14): 2041-2053. doi: 10.18186/thermal.1051307
15. Mozafary, B., Akbar, A., Arani, A., et al. (2024), *Brownian motion models effect on the nanofluid fluid flow and heat transfer in the natural, mixed, and forced convection*, J Ther. Eng. 10(1): 88-100. doi: 10.18186/thermal.1429382
16. Lee, S., Choi, S.U.S., Li, S., Eastman, J.A. (1999), *Measuring thermal conductivity of fluids containing oxide nanoparticles*, J Heat Transfer, 121(2): 280-289. doi: 10.1115/1.2825978
17. Hwang, K.S., Jang, S.P., Choi, S.U.S. (2009), *Flow and convective heat transfer characteristics of water-based Al_2O_3 nanofluids in fully developed laminar flow regime*, Int. J Heat Mass Transfer, 52(1-2): 193-199. doi: 10.1016/j.ijheatmasstransfer.2008.06.032
18. Godson, L., Raja, B., Mohan Lal, D., Wongwises, S. (2012), *Convective heat transfer characteristics of silver-water nanofluid under laminar and turbulent flow conditions*, J Thermal Sci. Eng. Appl. 4(3): 031001. doi: 10.1115/1.4006027
19. AbdEl-Gaied, S.M., Hamad, M.A.A. (2013), *MHD forced convection laminar boundary layer flow of alumina-water nanofluid over a moving permeable flat plate with convective surface boundary condition*, J Appl. Math. 2013: Art. ID 403210. doi: 10.1155/2013/403210
20. Pragya, Vasanthakumari, R. (2016), *Boundary layer flow of silver and titaniumoxide nanofluids over vertical stretching sheet*, Int. J Heat Technol. 34(3): 371-376. doi: 10.18280/ijht.340304
21. Khan, I., Alqahtani, A.M. (2019), *MHD nanofluids in a permeable channel with porosity*, Symmetry, 11(3): 378. doi: 10.3390/sym11030378
22. Elgazery, N.S. (2019), *Flow of non-Newtonian magneto-fluid with gold and alumina nanoparticles through a non-Darcian porous medium*, J Egypt. Math. Soc. 27(1): 39. doi: 10.1186/s42787-019-0017-x
23. Mahalakshmi, D., Vennila, B. (2020), *Boundary layer flow of silver and gold nanofluids over a flat plate by a domain decomposition method*, AIP Conf. Proc. 2277(1): 170002. doi: 10.1063/5.0025571
24. Klazly, M.M., Bognár, G. (2020), *Investigation of convective heat transfer enhancement for nanofluid flow over flat plate*, J Phys.: Conf. Ser., 1564(1): 012007. doi: 10.1088/1742-6596/1564/1/012007
25. Aminuddin, N.A., Nasir, N.A.A.M., Jamshed, W., et al. (2024), *Velocity and thermal slip impact towards GO-MoS_2/$C_3H_8O_3$ hybridity nanofluid flowing via a moving Riga plate*, Ain Shams Eng. J, 15(4): 102648. doi: 10.1016/j.asej.2024.102648
26. Pattnaik, P.K., Parida, S.K., Mishra, S.R., et al. (2022), *Analysis of metallic nanoparticles (Cu, Al_2O_3, and SWCNTs) on magnetohydrodynamics water-based nanofluid through a porous medium*, J Math. 2022(1): 3237815. doi: 10.1155/2022/3237815
27. Waqas, H., Fida, M., Liu, D., et al. (2022), *Heat transport of nanofluid flow through a porous channel with thermal radiation effects*, Int. Comm. Heat Mass Transfer, 138: 106376. doi: 10.1016/j.icheatmasstransfer.2022.106376
28. Gonsalves, S., Gabbur, S. (2023), *Finite element study of nanofluid through porous nonlinear stretching surface under convective boundary conditions*, Mater. Today: Proc. 2023, in press, corr. proof. doi: 10.1016/j.matpr.2023.07.277
29. Gonsalves, S., Gabbur, S. (2023), *Convective heat transfer of radiating magneto-micropolar nanofluid flow*, Int. J Heat Technol. 41(4): 959-968. doi.org/10.18280/ijht.410418
30. Jan, S.A.A., Ali, F., Sheikh, N.A., et al. (2018), *Engine oil based generalized brinkman-type nano-liquid with molybdenum disulphide nanoparticles of spherical shape: Atangana-Baleanu fractional model*, Numer. Meth. Part. Diff. Equat. 34(5): 1472-1488. doi: 10.1002/num.22200
31. Eswaraiah, V., Sankaranarayanan, V., Ramaprabhu, S. (2011), *Graphene-based engine oil nanofluids for tribological applications*, ACS Appl. Mater. Interfaces, 3(11): 4221-4227. doi: 10.1021/am200851z
32. Meng, Y., Su, F., Chen, Y. (2016), *Supercritical fluid synthesis and tribological applications of silver nanoparticle-decorated*

graphene in engine oil nanofluid, Sci. Rep. 6(1): 31246. doi: 10.1038/srep31246
33. Aman, S., Salleh, M.Z., Ismail, Z., Khan, I. (2017), *Exact solution for heat transfer free convection flow of Maxwell nanofluids with graphene nanoparticles*, J Phys.: Conf. Ser. 890(1): 012004. doi: 10.1088/1742-6596/890/1/012004
34. Arif, M., Ali, F., Sheikh, N.A., Khan, I. (2019), *Enhanced heat transfer in working fluids using nanoparticles with ramped wall temperature: Applications in engine oil*, Adv. Mech. Eng. 11 (11). doi: 10.1177/1687814019880987
35. Siddique, I., Sadiq, K., Jaradat, M.M.M., et al. (2022), *Engine oil based MoS_2 Casson nanofluid flow with ramped boundary conditions and thermal radiation through a channel*, Case Stud. Therm. Eng. 35: 102118. doi: 10.1016/j.csite.2022.102118
36. Le, Q.H., Ali, Q., Al-Khaled, K., et al. (2024), *Study of hybrid nanofluid containing graphene oxide and molybdenum disulfide nanoparticles with engine oil base fluid: A non-singular fractional approach*, Ain Shams Eng. J, 15(1): 102317. doi: 10.1016/j.asej.2023.102317
37. Gonsalves, S., Gabbur, S. (2023), *Heat transfer analysis using finite element method under convective boundary condition*, E3S Web of Conf. 430: 01248. doi: 10.1051/e3sconf/202343001248
38. Oztop, H.F., Abu-Nada, E. (2008), *Numerical study of natural convection in partially heated rectangular enclosures filled with nanofluids*, Int. J Heat Fluid Flow, 29(5): 1326-1336. doi: 10.1016/j.ijheatfluidflow.2008.04.009
39. Devi, S.A., Andrews, J. (2011), *Laminar boundary layer flow of nanofluid over a flat plate*, Int. J Appl. Math. Mech, 7(6): 52-71.
40. Reddy, J.N., Introduction to the Finite Element Method, 4th Ed., McGraw-Hill Education, New York, 2019. ISBN: 978125 9861901
41. Roşca, N.C., Pop, I. (2014), *Unsteady boundary layer flow of a nanofluid past a moving surface in an external uniform free stream using Buongiorno's model*, Comp. Fluids, 95: 49-55. doi: 10.1016/j.compfluid.2014.02.011

Nomenclature

a	convective boundary parameter
x, y	coordinates along and orthogonal to the plate
f	dimensionless stream function
u, v	velocity components (ms^{-1})
q	dimensionless velocity
s_w	suction parameter
T	temperature (K)
h_f	heat transfer coefficient

Greek symbols

θ	dimensionless temperature
ϕ	solid (nanoparticles) volume fraction
k	thermal conductivity ($WK^{-1}m^{-1}$)
ρ	density ($kg{\cdot}m^{-3}$)
μ	viscosity (m^2s^{-1})
ρC_p	heat capacity
ρ_f	density of base fluid ($kg{\cdot}m^{-3}$)
ν_f	viscosity of base fluid (m^2s^{-1})
η	dimensionless coordinate

Subscripts

y	1st order partial differentiation with respect to y
x	1st order partial differentiation with respect to x
yy	2nd order partial differentiation with respect to y
f	base fluid
nf	nanofluid
m, n	matrix dimensions

Superscript

$'$	differentiation with respect to η

Acronyms

FEM	finite element method
ODE	ordinary differential equation
PDE	Partial differential equations